Organic Electronics 13 (2012) 959–968

Contents lists available at SciVerse ScienceDirect

Organic Electronics

journal homepage: www.elsevier.com/locate/orgel

Solution processed WO_3 layer for the replacement of PEDOT:PSS layer in organic photovoltaic cells

Hana Choi [a,b], BongSoo Kim [a], Min Jae Ko [a], Doh-Kwon Lee [a], Honggon Kim [a], Sung Hyun Kim [b,*], Kyungkon Kim [a,c,*]

[a] Solar Cell Research Center, Korea Institute of Science and Technology, Seongbuk-gu, Seoul 136-713, Republic of Korea
[b] Energy and Environmental Lab, Department of Chemical and Biological Engineering, Korea University, Seongbuk-gu, Seoul 136-701, Republic of Korea
[c] Department of Chemistry and Nano Science, Division of Molecular and Life Sciences, College of Natural Sciences, Ewha Womans University, 52, Ewhayeodae-gil, Seodaemun-gu, Seoul, Republic of Korea

ARTICLE INFO

Article history:
Received 3 August 2011
Received in revised form 30 January 2012
Accepted 31 January 2012
Available online 24 February 2012

Keywords:
Organic photovoltaic cells
Hole extraction layer
Metal oxide
Device stability

ABSTRACT

Tungsten oxide layer is formed uniformly by a sol–gel technique on top of indium tin oxide as a neutral and photo-stable hole extraction layer (HEL). The solution processed tungsten oxide layer (sWO_3) is fully characterized by UV–Vis, XPS, UPS, XRD, AFM, and TEM. Optical transmission of ITO/sWO_3 substrates is nearly identical to ITOs. In addition, the sWO_3 layer induces nearly ohmic contact to P3HT as PEDOT:PSS layer does, which is determined by UPS measurement. In case that an optimized thickness (~10 nm) of the sWO_3 layer is incorporated in the organic photovoltaic devices (OPVs) with a structure of ITO/sWO_3/P3HT:PCBM/Al, the power conversion efficiency (PCE) is 3.4%, comparable to that of devices utilizing PEDOT:PSS as HEL. Furthermore, the stability of OPV utilizing sWO_3 is significantly enhanced due to the air- and photo-stability of the sWO_3 layer itself. PCEs are decreased to 40% and 0% of initial values, when PEDOT:PSS layers are exposed to air and light for 192 h, respectively. In contrast, PCEs are maintained to 90% and 87% of initial PCEs respectively, when sWO_3 layers are exposed to the same conditions. Conclusively, we find that solution processed tungsten oxide layers can be prepared easily, act as an efficient hole extraction layer, and afford a much higher stability than PEDOT:PSS layers.

1. Introduction

Organic photovoltaic (OPV) cells have attracted great interest as a promising candidate for future green energy resource because they can be applied to flexible, light-weighted, low-cost, and large-area applications using cost-effective solution processing such as roll-to-roll [1–3]. Power conversion efficiencies (PCE) of OPV cells composed of poly(3-hexylthiophene) (P3HT) and [6,6]-phenyl-C61-butyric acid methyl ester (PCBM) were reported to be 4–5% previously [4]. Recently OPVs incorporating low band gap polymers as electron donors have reached more than 8% PCEs [5,6]. Inspite of this substantial progress in PCEs, however, it is strongly needed to improve device stability for commercialization. In addition, for the large scale and high throughput production of OPVs, it is desirable to generate all functional layers by solution processing [7–9].

Intensive studies have been carried out to understand degradation mechanisms [10,11] and improve the stability of OPVs [12,13]. Representative degradation pathways include photo-degradation of organic materials [14,15], gradually proceeding phase separation in the active film [16–18], oxidation of metal electrode (e.g. Al_2O_3 formation) [19,20], and instability of poly(ethylenedioxythiophene) doped with poly(styrenesulfonate) (PEDOT:PSS) [21–23] in the conventional type solar cell. Especially, the

* Corresponding authors. Address: Solar Cell Research Center, Korea Institute of Science and Technology, Seongbuk-gu, Seoul 136-713, Republic of Korea (K. Kim). Tel.: +82 02 32903297; fax: +82 02 9266102 (S.H. Kim), tel.: +82 02 9585362; fax: +82 02 9585309 (K. Kim).
E-mail addresses: kimsh@korea.ac.kr (S.H. Kim), kimkk@kist.re.kr (K. Kim).

1566-1199/$ - see front matter © 2012 Elsevier B.V. All rights reserved.
doi:10.1016/j.orgel.2012.01.033

PEDOT:PSS layer causes several detrimental effects. First, the PEDOT:PSS is highly hygroscopic. When the PEDOT:PSS layer absorbs water, its conductivity decreases and thus device lifetime shortens [23–25]. Secondly, the PEDOT:PSS layer is highly acidic (a measured pH of 1.2) [26]. Chemical degradation occurs at the interface between ITO and PEDOT:PSS in the presence of water. Third, the PEDOT:PSS is known to be easily photo-oxidized [22,27].

In order to replace this problematic PEDOT:PSS layer, several metal oxides such as V_2O_5 [28], MoO_3 [28,29], NiO [30], and WO_3 [31,32] have been employed as a HEL in OPVs. OPV cells using such layers showed comparable efficiencies to those using the PEDOT:PSS layer. Moreover, they are advantageous over the PEDOT:PSS layer since they are neutral, chemically stable, and photo-stable. However, these metal oxide layers have so far been predominantly accessible via sputtering, thermal evaporation, and pulsed laser deposition, which methods are neither scalable nor cost effective. There are only a few reports of solution processed CuO_x [33], NiO [8] and V_2O_5 [7] as HELs in OPVs.

In this article, we explore a new kind of solution-processed WO_3 (sWO_3) layer as HEL. Uniform sWO_3 layers were prepared in a controlled manner. The sWO_3 layer allows us to fabricate devices with a structure of ITO/sWO_3/P3HT:PCBM/Al, whose PCE is comparable to that of devices employing the PEDOT:PSS layer. Further, we observed considerably improved air/photo-stability of devices compared to the PEDOT:PSS layer.

2. Experimental

2.1. PEDOT:PSS coated ITO substrates

ITO glass substrates were cleaned using the following sequential steps: rinsing with deionized water; sonication in warm acetone, and isopropanol for 10 min each; and drying under a stream of nitrogen. Finally, the substrates were treated with UV ozone for 20 min before spin-coating PEDOT:PSS layer. PEDOT:PSS solution was purchased from Clevios (AI4083, Germany) and diluted with methanol by 1:1 vol.%. The resulting solution generated a 30 nm-thick PEDOT:PSS layer on spin-coating at a speed of 4000 rpm for 35 s. The PEDOT:PSS coated ITO substrates were dried in a vacuum oven at 120 °C for 10 min.

2.2. Solution processed WO_3 (sWO_3) coated ITO substrates

ITO glass substrates cleaned as described above were inserted into glove box. 0.1 M of tungsten ethoxide [$W(OC_2H_5)_6$] with an analytic purity of 99.9% (CHEMAT

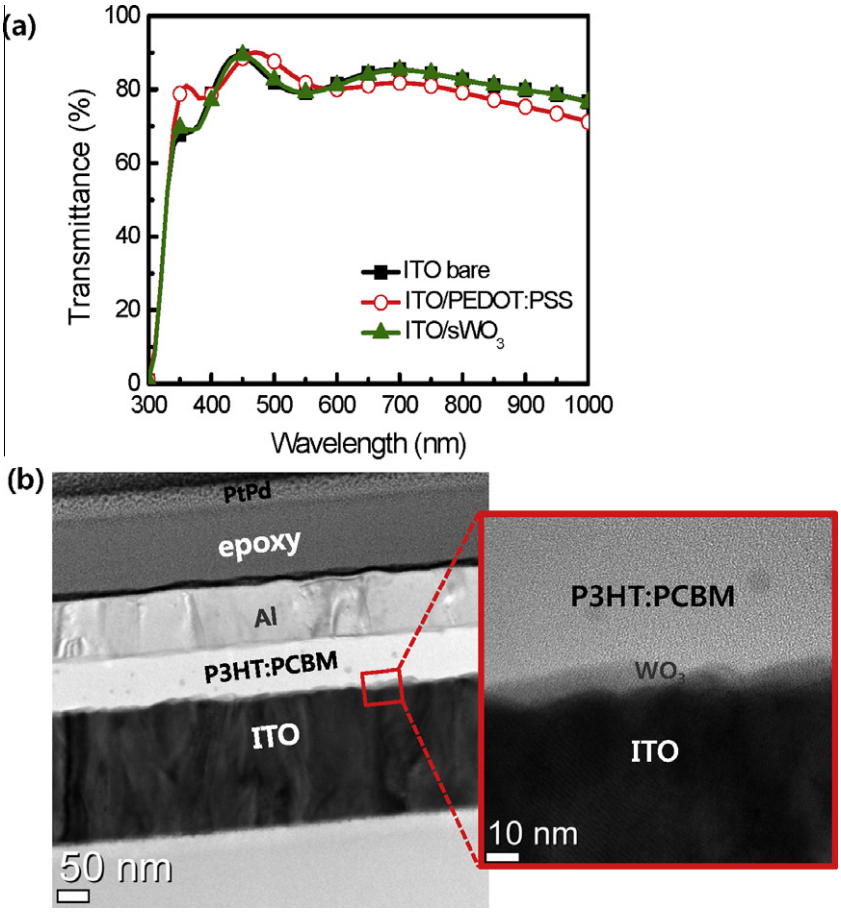

Fig. 1. (a) Optical transmission spectra of ITO/sWO_3, ITO/PEDOT:PSS and bare ITO substrates. (b) TEM cross-sectional image of ITO/sWO_3/P3HT:PCBM/Al device.

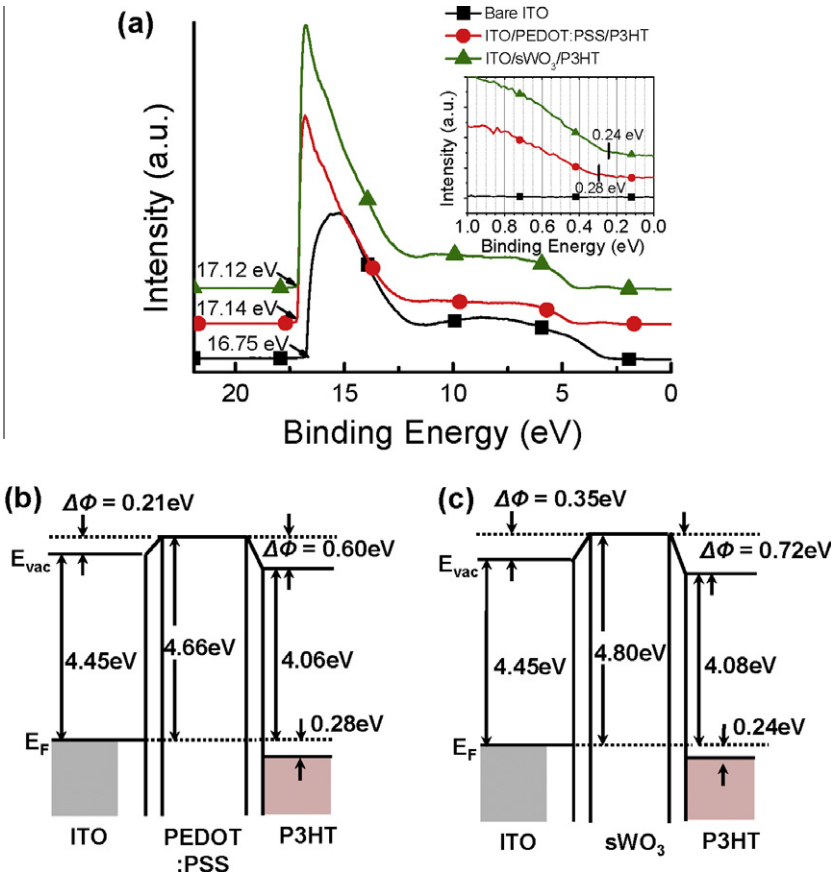

Fig. 2. (a) UPS spectra of bare ITO, ITO/PEDOT:PSS/P3HT, and ITO/sWO_3/P3HT. The inset shows the region of HOMO band of P3HT film. Arrows indicate secondary electron cut-off of films or the onset of the HOMO band of P3HT film. (b) Energy level diagram of ITO/PEDOT:PSS/P3HT. (c) Energy level diagram of ITO/sWO_3/P3HT. Arrows indicate energy gaps; E_{vac} indicates vacuum level, E_F Fermi level, and $\Delta\Phi$ work function change.

TECHNOLOGY Inc., USA) was purchased. The tungsten oxide solution was diluted with ethanol into various concentrations inside glove box and the diluted solutions were then used to spin-coat ITO substrates at a speed of 4000 rpm for 40 s. The thickness of the sWO_3 films was controlled by the concentration of tungsten ethoxide solution. sWO_3 films were stored in air overnight to complete the hydrolysis and condensation reactions.

2.3. OPV cell fabrication and property measurement

P3HT and PCBM blended solution was used to form bulk-heterojunction active layers for solar cell devices. P3HT and PCBM (used as received from Rieke Metals and Nano-C, respectively) were dissolved in chlorobenzene with the weight ratio of 1:0.8 at a polymer concentration of 1 mg/mL and homogenized for 4 h. The P3HT:PCBM solution is then spin-coated onto ITO/HEL substrates at 1000 rpm for 15 s and dried at room temperature for 10 min in air. After transferring ITO/HEL/P3HT:PCBM films into a vacuum chamber, 100 nm thick aluminum was vacuum deposited in the base pressure of 2×10^{-6} Torr at a deposition rate of 5 Å/s through a shadow mask. Afterward, devices are post-annealed at 145 °C for 10 min by a radiation heater inside the vacuum chamber. Current density versus voltage (J–V) characteristic were recorded on a Keithley model 2400 source measuring unit. A class-A solar simulator with a 150 W Xenon lamp (Newport) equipped with a KG-3 filter served as a light source. Its light intensity was adjusted to AM 1.5 G 1 sun light intensity using a NREL-calibrated mono Si solar cell. External quantum efficiency (EQE) was measured as a function of wavelength from 300 to 800 nm on incident photo-to-current conversion equipment (PV measurement Inc.). Calibration was performed using a silicon photodiode G425, which is NIST-calibrated as a standard.

2.4. Thin film characterization

Absorbance and reflectance spectra were recorded on a Perkin–Elmer Lambda 35 UV/Vis spectrometer. The cross-sectional image of the device was taken on the Dual Beam FIB/SEM system (Helios 600, FEI Company), which allows sectional analysis for the cross-section of delaminated region. X-ray diffraction (XRD) spectra were recorded at room temperature on a RIGAKU X-ray diffractometer using Cu K_α radiation (λ = 1.5406 Å) at operating power of 40 kV and 300 mA. The XPS and UPS measurements were

performed with monochromatized Al K_α X-ray photons ($h\nu$ = 1486.6 eV for XPS) and He I (21.2 eV for UPS) discharge lamp using an AXIS–NOVA System (Kratos Inc.) under high vacuum (1×10^{-9} Torr). For XPS, the binding energies were corrected by reference to the (C1s) line at 284.6 kV. For UPS, a sample bias of −15 V was used in order to separate the sample and the secondary edge for analyzer. All samples were kept inside a high-vacuum chamber overnight. The surface morphology of sWO_3 on ITO substrates was imaged using an atomic force microscopy (AFM, XE-100, Park Systems) on AC160-TS cantilever in the tapping mode.

3. Results and discussion

sWO_3 films were spin-coated at room temperature from various concentrations of tungsten ethoxide precursor solutions on cleaned ITO substrates. The resulting sWO_3 films were stored in air overnight to complete hydrolysis and condensation reactions [34], which were then fully characterized. Note that we found that an optimized tungsten ethoxide solution concentration for ITO/sWO_3/P3HT:PCBM/Al devices was 0.007 M (~10 nm). Unless we specify solution concentration, sWO_3 denotes films spin-coated from 0.007 M solution. PEDOT:PSS-coated ITO (ITO/PEDOT:PSS) substrates were also used for comparison purpose for most characterization.

We first measured light transmittance of ITO/sWO_3, ITO/PEDOT:PSS, and ITO substrates. Transmission spectra are shown in Fig. 1(a). ITO/sWO_3 substrates show nearly the same transmittance as ITO substrates with a maximum value of 89% at 450 nm. Importantly, ITO/sWO_3 substrates show even higher transmittance than ITO/PEDOT:PSS substrates in the longer wavelength region (>580 nm). This suggests that ITO/sWO_3 substrates are suitable for OPV cells especially utilizing low band gap materials.

We also conducted transmission electron microscopy (TEM) imaging on the cross-section of the ITO/sWO_3/P3HT:PCBM/Al device. TEM cross-sectional image in Fig. 1(b) shows that the sWO_3 film forms conformal coating on the ITO surface, and its thickness was estimated to be approximately 10 nm. Moreover, we examined the roughness of sWO_3 film on ITO (ITO/sWO_3) as well as other substrates, PEDOT:PSS-coated ITO (ITO/PEDOT:PSS) and bare ITO by tapping mode atomic force microscopy (TM-AFM). The R_{rms} roughness of ITO/sWO_3 was reduced to 3.83 nm compared to that of bare ITO (5.19 nm) and the

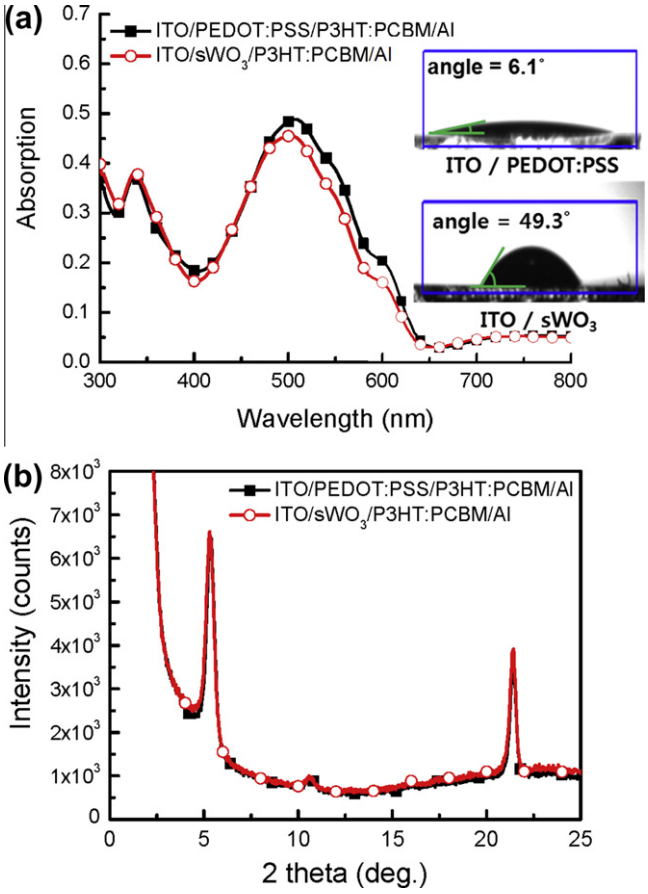

Fig. 3. (a) UV–Vis absorption spectra of annealed P3HT:PCBM films on the ITO/sWO_3 and ITO/PEDOT:PSS substrates and water-contact angle on these substrates. (b) X-ray diffraction spectra of P3HT:PCBM films on the ITO/sWO_3 and ITO/PEDOT:PSS substrates. P3HT:PCBM films were annealed at 145 °C for 10 min.

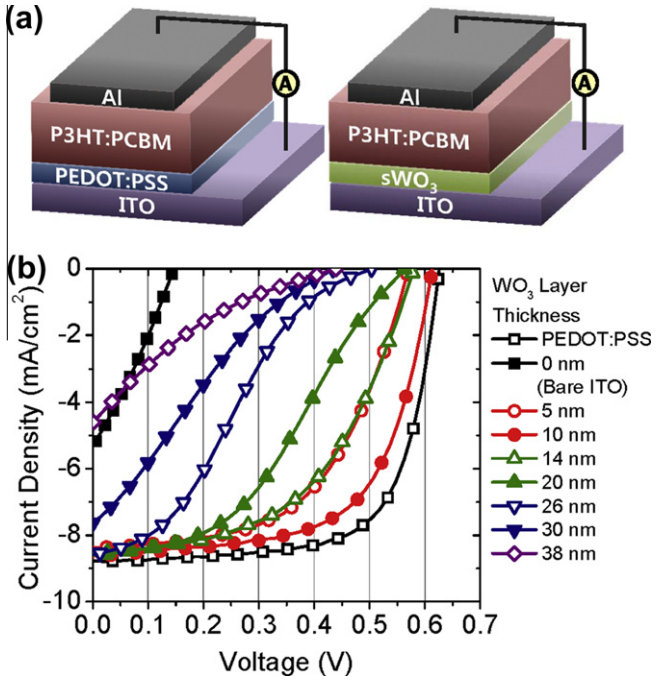

Fig. 4. (a) Schematic diagram of P3HT:PCBM bulk heterojunction cell structures using ITO/PEDOT:PSS and ITO/sWO_3 substrates. (b) Current density–voltage curves of solar cells employing various thickness of sWO_3 layers and PEDOT:PSS layer as hole extraction layers. Solar cells measured under 1 sun illumination (AM 1.5 G, 100 mW/cm^2).

value is slightly larger than that of PEDOT:PSS layer coated ITO (R_{rms} = 2.51 nm) (TM-AFM height images are shown in Fig. S.1). These observations suggest that tungsten ethoxide precursor planarized the rough ITO surface well.

In addition, we determined energy level alignment and work functions of each layer in the ITO/sWO_3/P3HT and ITO/PEDOT:PSS/P3HT using ultraviolet photoelectron spectroscopy (UPS). For the UPS measurement, 7 nm thick P3HT polymer film was formed on the ITO/PEDOT:PSS and ITO/sWO_3 substrates by spin-coating. The UPS measurements were performed with He I (21.2 eV) discharge lamp using an AXIS–NOVA System (Kratos Inc.). All samples were kept inside a high-vacuum chamber overnight. Fig. 2(a) shows UPS spectra of ITO/sWO_3/P3HT, and ITO/PEDOT:PSS/P3HT, and bare ITO. Fig. 2(a) (inset) clearly shows the positions of HOMO band onset of P3HT, which are 0.24 eV and 0.28 eV for ITO/sWO_3/P3HT, and ITO/PEDOT:PSS/P3HT, respectively. Compared to the energy gap of 0.34 eV upon direct contact of P3HT on ITO (Fig. S.3), these lower energy gaps between ITO and P3HT are constructed by interface dipole formation at each interface, accompanying work function changes as shown in Fig. 2(b) and (c). Therefore, the incorporation of these HELs in devices create nearly ohmic contact for hole extraction.

We next examined annealed P3HT:PCBM films on the ITO/HEL substrates using UV–Vis spectrometer and X-ray diffractometer. Fig. 3(a) shows that light absorption feature of annealed P3HT:PCBM films is very similar, but the absorptivity is slightly lower for the films on ITO/sWO_3 substrates in the wavelength region of 470–650 nm. The lower light absorption is probably because of the different directional orientation of crystalline P3HT polymer domains at the interface of the HELs as we observed two different surface energies from contact angle measurement (Fig. 3(a), inset) [35–38], and also because of slightly lower substrate transmission in those wavelengths (see Fig. 1(a)). Fig. 3(b) shows X-ray diffraction spectra of annealed P3HT:PCBM films on both ITO/PEDOT:PSS and ITO/sWO_3 where we found two typical diffraction peaks of (100)

Table 1
Device characteristics of P3HT:PCBM devices employing various thicknesses of sWO_3 layers as well as PEDOT:PSS layer under AM 1.5 G 1 sun light intensity of 100 mW/cm^2.

	V_{OC} (V)	J_{SC} (mA/cm^2)	*FF*	*PCE* (%)
ITO/P3HT:PCBM/Al	0.18	5.52	0.27	0.27
ITO/PEDOT:PSS/ P3HT:PCBM/Al	0.63	8.78	0.69	3.77
ITO/5 nm sWO_3/ P3HT:PCBM/Al	0.57	8.38	0.55	2.63
ITO/10 nm sWO_3/ P3HT:PCBM/Al	0.62	8.63	0.63	3.37
ITO/14 nm sWO_3/ P3HT:PCBM/Al	0.58	8.55	0.51	2.56
ITO/20 nm sWO_3/ P3HT:PCBM/Al	0.56	8.61	0.41	1.97
ITO/26 nm sWO_3/ P3HT:PCBM/Al	0.51	8.59	0.28	1.22
ITO/30 nm sWO_3P3HT:PCBM/Al	0.44	7.63	0.21	0.71
ITO/38 nm sWO_3/ P3HT:PCBM/Al	0.44	4.62	0.16	0.33

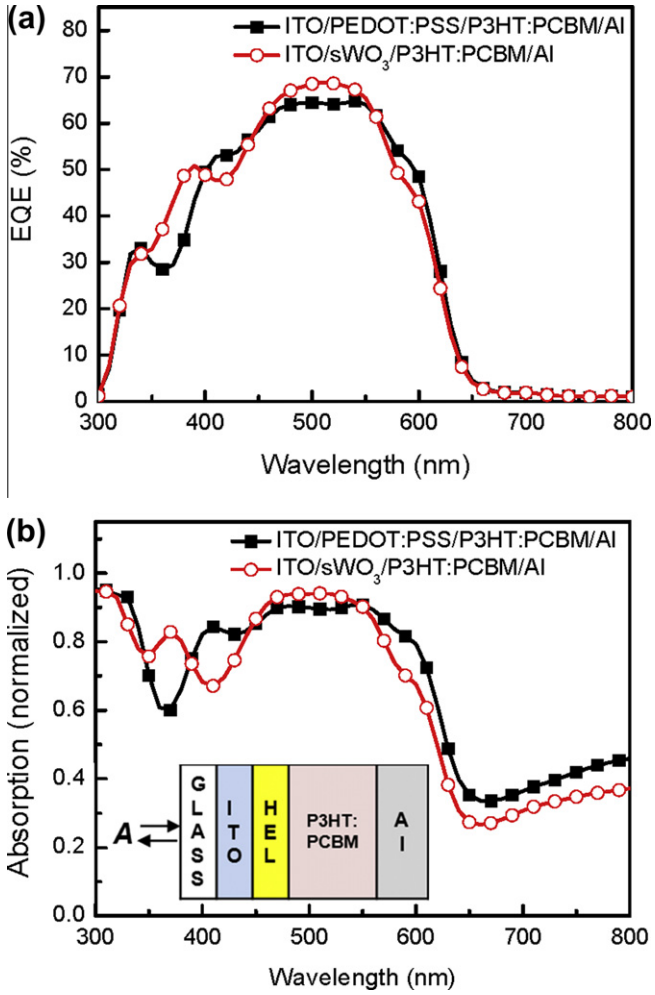

Fig. 5. (a) EQE spectra of ITO/PEDOT:PSS/P3HT:PCBM/Al device and ITO/sWO_3/P3HT:PCBM/Al devices. (b) Light absorption of devices with the structure of glass/ITO (180 nm)/PEDOT:PSS (30 nm)/P3HT:PCBM (80 nm)/Al (100 nm) and glass/ITO (180 nm)/sWO_3 (10 nm)/P3HT:PCBM (80 nm)/Al (100 nm), measured in the reflective mode.

and (200). X-ray diffraction pattern is independent of hole extraction layers. From UV–Vis and X-ray diffraction spectra, we concluded that film state of annealed P3HT:PCBM layers on either hole extraction layers are nearly the same, which is consistent with similar initial photovoltaic properties (shown below).

After analyzing sWO_3 layers and P3HT:PCBM films, photovoltaic performance of ITO/sWO_3/P3HT:PCBM/Al devices were measured as a function of sWO_3 film thickness (or solution concentration) under AM 1.5 G 1 sun light intensity of 100 mW/cm^2. In addition, photovoltaic performance of ITO/PEDOT:PSS/P3HT:PCBM/Al devices were measured for comparison (Fig. 4(a)). For device fabrication, P3HT and PCBM (1:0.8) blend solution was spin-coated on top of ITO/sWO_3 and ITO/PEDOT:PSS substrates to form bulk-heterojunction (BHJ) active layers. Aluminum was then evaporated for the completion of photovoltaic devices and post-annealing (145 °C for 10 min) on devices was followed. Fig. 4(b) shows photo-current density (J) versus voltage (V) curves of P3HT:PCBM BHJ devices and Table 1 summarizes device characteristics. OPV devices without and with the 10 nm thick sWO_3 layer give rise to a significant increase in J_{SC} from 5.52 mA/cm^2 to 8.57 mA/cm^2 respectively and in V_{OC} from 0.18 V to 0.62 V respectively, resulting in a remarkable PCE increase from 0.27% to 3.37%. This indicates that the sWO_3 layer effectively prevents the recombination of charge carriers at the organic/ITO interface [32]. The lower concentration solutions failed to cover rough ITO surface uniformly, and higher concentration solutions resulted into thick films. It is well known that the *FF* of solar cell is closely related to the internal resistance of the device. The *FF* and J_{SC} of solar cell will be decreased as the series resistance is increased. The tendency is ascribed to low electrical conductivity of the sWO_3 film (conductivity dependence of thickness of sWO_3 films are provided in Table S.1). The sWO_3 films thicker than 10 nm create higher series resistances and thus lower J_{SC} and *FF* values. Moreover, when the device PCE using sWO_3 layers prepared from 0.007 M tungsten ethoxide solution is compared with the device PCE using

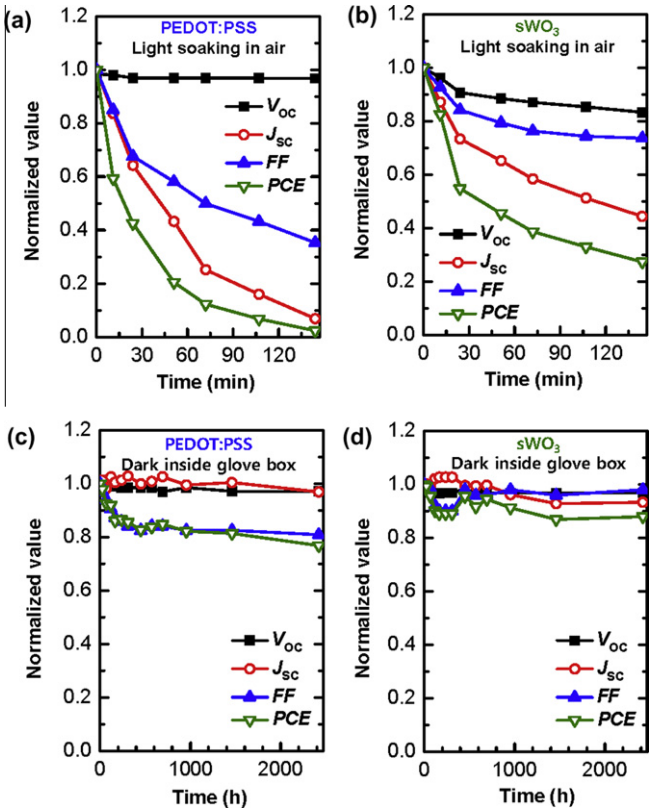

Fig. 6. (a, b) Cell stability of ITO/HEL/P3HT:PCBM/Al devices using PEDOT:PSS and sWO_3 layers, respectively, stored in air under continuous light soaking condition. (c, d) Cell stability of ITO/HEL/P3HT:PCBM/Al devices using PEDOT:PSS and sWO_3 layers, respectively, stored inside glove box under dark condition. Devices were not encapsulated.

PEDOT:PSS layers, PCEs are nearly the same (Fig. 4(b)). This suggests that the 10 nm thick sWO_3 layer is one of good alternatives for the replacement of the PEDOT:PSS layer.

We also carried out external quantum efficiency (EQE) experiments under a monochromatic beam generated by a 75 W Xenon light to understand the origin of the similar J_{SC} from two different hole extraction layers of sWO_3 and PEDOT:PSS. Fig. 5(a) shows EQE spectra of P3HT:PCBM devices using ITO/sWO_3 and ITO/PEDOT:PSS substrates. From these EQE spectra, we estimated J_{SC} corresponding to 8.55 mA/cm^2 and 8.54 mA/cm^2 for ITO/sWO_3 and ITO/PEDOT:PSS substrates, respectively, which are consistent with the above result under AM 1.5 G 1 sun light intensity of 100 mW/cm^2. Although the integrated J_{SC} values are the same, each EQE value as function of wavelength is dependent on the kind of HEL. Compared to devices with the PEDOT:PSS layer, EQE values of devices using the sWO_3 layer are higher in the range of 350–400 nm and 450–500 nm than those of devices using the PEDOT:PSS layer. This result cannot be explained simply by the transmittance of each ITO/HEL substrate and UV–Vis absorption (Figs. 1(a) and 3(a)). To find the origin of the difference in the two types of devices, we measured light absorption of devices in the reflective mode. Fig. 5(b) clearly shows that light absorption spectra measured in the reflective mode are well matched with EQE spectral shape. Therefore, the difference is attributed primarily to redistribution of the light intensity within the active layer in the device. This may be due to high refractive index of WO_3 compared with PEDOT:PSS and the different thicknesses.

We lastly measured device stabilities under various conditions. Fig. 6(a) and (b) showed cell stability data of P3HT:PCBM devices using ITO/PEDOT:PSS and ITO/sWO_3 substrates, respectively, stored in air under continuous light soaking condition. The light intensity of the lamp is adjusted to the 1 sun light intensity of 100 mW/cm^2 and continuous light was applied to the devices. Devices were not encapsulated for stability test. Temperature inside the testing chamber was kept at 35 °C. In this condition, devices based on both ITO/PEDOT:PSS and ITO/sWO_3 substrates undergo rapid degradation. After 144 min, the PCE of the former substrate was decreased to nearly 0% of the initial PCE and that of the latter 27%. J_{SC} reduction as well as *FF* is manifest while the sWO_3 layer helps maintain slightly higher. Fig. 6(c) and (d) shows cell stability test results of P3HT:PCBM devices using ITO/PEDOT:PSS and ITO/sWO_3 substrates respectively, stored inside glove box under dark condition. Unlike devices stored in air, both types of devices were much stable over 2500 h. PEDOT:PSS-based and sWO_3-based devices maintain 77% and 88% of

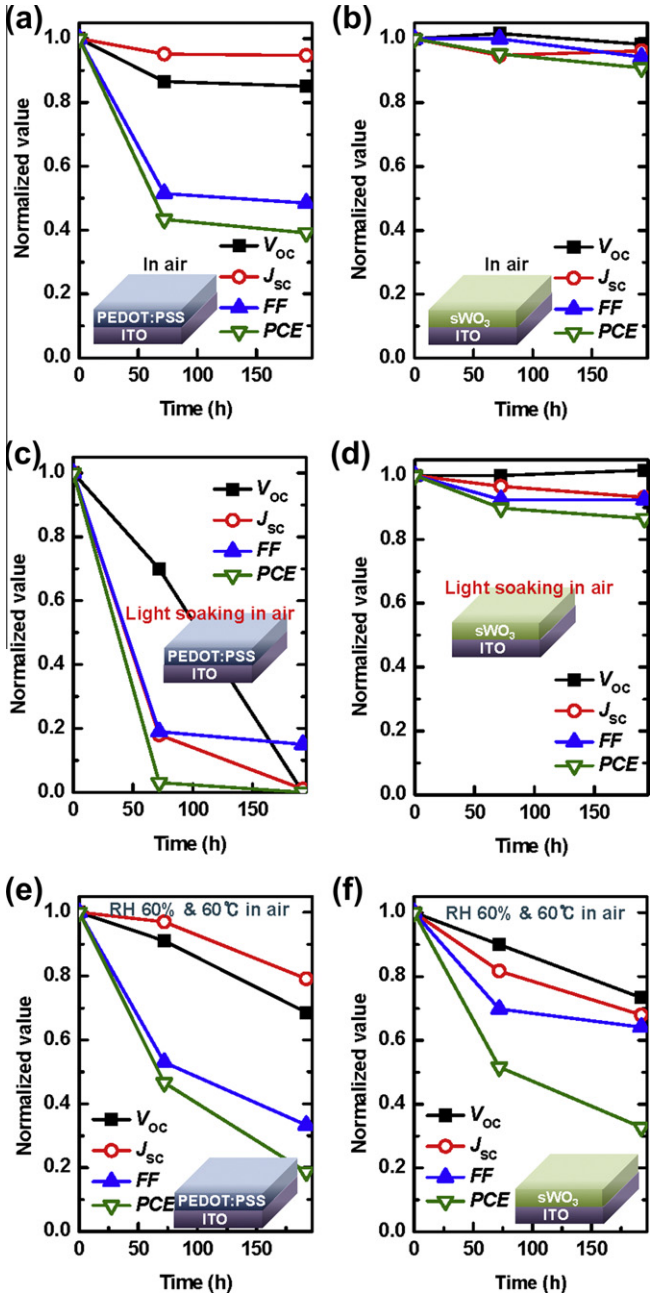

Fig. 7. (a, b) Cell stability of ITO/HEL/P3HT:PCBM/Al devices using PEDOT:PSS and sWO_3 layers stored in air for 192 h, respectively. (c, d) Cell stability of ITO/HEL/P3HT:PCBM/Al devices using PEDOT:PSS and sWO_3 layers stored in air under light soaking condition for 192 h respectively. (e, f) Cell stability of ITO/HEL/P3HT:PCBM/Al devices using PEDOT:PSS and sWO_3 layers stored under RH 60% at 60 °C condition for 192 h, respectively.

the initial PCE, respectively. The slight PCE reduction in the initial period (up to ~250 h) could be mainly caused by residual air/H_2O in the PEDOT:PSS and active layers, which resulted in increased series resistance and reduced fill factor.

These results reflect that the sWO_3 layer is much more stable than the PEDOT:PSS layer in the above conditions. However, it is known that air and light exposure triggers degradation such as: (i) photo-oxidation and chemical degradation of HELs, (ii) photo-degradation of active layers, and (iii) oxidation of metal/active interfaces [22–27]. Therefore, in order to discern the effect of different HELs on the device stability, we studied the stability of the PEDOT:PSS and sWO_3 layers more specifically. The PEDOT:PSS and sWO_3 layers were exposed to air only, air/light soaking, and humid/temperature (RH 60% at 60 °C) conditions, which were then used as HELs of OPV devices.

Fig. 7(a) and (b) shows the stability test result of devices based on air-exposed HELs. We found that the PEDOT:PSS layer is much more vulnerable to air exposure than the

sWO_3 layer. 192 h air exposure on the PEDOT:PSS layer lead to 61% PCE decrease mainly due to *FF* decrease. That is, the degradation of the PEDOT:PSS layer results in the considerable increase of series resistance. Over the same period, the sWO_3 layer showed only 9% PCE decrease. Fig. 7(c) and (d) shows the stability test result of devices based on air/continuous light exposed HELs. We found that the degradation of the PEDOT:PSS layer was accelerated while the sWO_3 layer was much more robust to continuous light. The PCE based on the PEDOT:PSS layer was decreased to nearly 0% of the initial PCE after only 70 h with significant reduction in all parameters, J_{SC}, V_{OC}, and *FF*, indicating light soaking in air makes PEDOT:PSS layers deteriorated rapidly. The degradation mechanism of the PEDOT:PSS layer is related to photochemical oxidation of the PEDOT:PSS layer [22,27], i.e., the PEDOT:PSS layer can be oxidized by oxygen under light and lose its conductivity. On the contrary, the PCE based on the sWO_3 layer was slightly reduced by 13% of the initial PCE after 192 h, similarly to just air exposure condition. Further, Fig. 7(e) and (f) shows the stability test result of devices based on HELs stored with RH 60% at 60 °C in air. Here again we found that the sWO_3 layer is more stable than the PEDOT:PSS layer with the PCE decreases to 33% and 29%, respectively. The difference of PCE decrease behavior is related to the hydrophilicity of the HELs as found in contact angle measurement in Fig. 3(a). From all data in Fig. 7, we concluded that the PEDOT:PSS layer is quite sensitive to air, light, and humidity and the sWO_3 layer is highly stable in air and light but weak to humidity.

These stability results in Figs. 6 and 7 provide important implications: (i) air, light, and humidity/temperature play a critical role in degradation and thus proper encapsulation of devices is essential to guarantee device stability, (ii) the sWO_3 layer is much more stable when exposed to air and light than the PEDOT:PSS layer, and (iii) therefore, the sWO_3 layer would be an excellent substitute for the PEDOT:PSS layer.

4. Conclusion

We have developed solution-processed tungsten oxide layer (sWO_3) for the efficient and stable hole extraction layer in the OPV devices. We found several merits of this sWO_3 layer including (i) easy film formation at room temperature, (ii) high optical transmittance over wide solar spectral range, (iii) proper energy level alignment for hole extraction from P3HT. Moreover, when incorporated in P3HT:PCBM devices, the sWO_3 layer shows comparable efficiency to the PEDOT:PSS layer. Further, we demonstrate substantial improvement in device stability due to the environmental stability of the sWO_3 layer. Therefore, we believe that the sWO_3 layer is a promising hole extraction layer to replace the PEDOT:PSS layer in OPV devices.

Acknowledgements

This research was supported by New and Renewable Energy Program through the Korea Institute of Energy Technology Evaluation and Planning (KETEP) funded by the Ministry of Knowledge Economy (MKE) (008NPV08J010000), the Pioneer Research Center Program through the National Research Foundation of Korea funded by the Ministry of Education, Science and Technology (2009-0081500) and Industry Resource Technology Development Program (Contract: 10034648) from Korea Ministry of Knowledge and Economy.

Appendix A. Supplementary data

Supplementary data associated with this article can be found, in the online version, at doi:10.1016/j.orgel.2012.01.033.

References

[1] K.X. Steirer, J.J. Berry, M.O. Reese, M.F.A.M. van Hest, A. Miedaner, M.W. Liberatore, R.T. Collins, D.S. Ginley, Thin Solid Films 517 (2009) 2781.
[2] S.E. Shaheen, R. Radspinner, N. Peyghambarian, G.E. Jabbour, Appl. Phys. Lett. 79 (2001) 2996.
[3] F.C. Krebs, S.A. Gevorgyan, J. Alstrup, J. Mater. Chem. 19 (2009) 5442.
[4] G. Li, V. Shrotriya, J.S. Huang, Y. Yao, T. Moriarty, K. Emery, Y. Yang, Nat. Mater. 4 (2005) 864.
[5] Y. Liang, Z. Xu, J. Xia, S.-T. Tsai, Y. Wu, G. Li, C. Ray, L. Yu, Adv. Mater. 22 (2010) E135.
[6] R.F. Service, Science 332 (2011) 293.
[7] K. Zilberberg, S. Trost, H. Schmidt, T. Riedl, Adv. Energy Mater. 1 (2011) 377.
[8] K.X. Steirer, J.P. Chesin, N.E. Widjonarko, J.J. Berry, A. Miedaner, D.S. Ginley, D.C. Olson, Org. Electron. 11 (2010) 1414.
[9] J. Meyer, R. Khalandovsky, P. Görrn, A. Kahn, Adv. Mater. 23 (2011) 70.
[10] F.C. Krebs, K. Norrman, Prog. Photovoltaics 15 (2007) 697.
[11] M. Jorgensen, K. Norrman, F.C. Krebs, Sol. Energy Mater. Sol. Cells 92 (2008) 686.
[12] D.H. Wang, S.H. Im, H.K. Lee, O.O. Park, J.H. Park, J. Phys. Chem. C 113 (2009) 17268.
[13] K. Lee, J.Y. Kim, S.H. Park, S.H. Kim, S. Cho, A.J. Heeger, Adv. Mater. 19 (2007) 2445.
[14] K.Z. Xing, N. Johansson, Adv. Mater. 9 (1997) 1027.
[15] A. Kumar, R. Devine, C. Mayberry, B. Lei, G. Li, Y. Yang, Adv. Funct. Mater. 20 (2010) 2729.
[16] B.J. Kim, Y. Miyamoto, B.W. Ma, J.M.J. Frechet, Adv. Funct. Mater. 19 (2009) 2273.
[17] K. Sivula, Z.T. Ball, N. Watanabe, J.M.J. Frechet, Adv. Mater. 18 (2006) 206.
[18] S. Gunes, H. Neugebauer, N.S. Sariciftci, Chem. Rev. 107 (2007) 1324.
[19] M.T. Lloyd, D.C. Olson, P. Lu, E. Fang, D.L. Moore, M.S. White, M.O. Reese, D.S. Ginley, J.W.P. Hsu, J. Mater. Chem. 19 (2009) 7638.
[20] K. Norrman, S.A. Gevorgyan, F.C. Krebs, ACS Appl. Mater. Interf. 1 (2009) 102.
[21] E. Vitoratos, S. Sakkopoulos, E. Dalas, N. Paliatsas, D. Karageorgopoulos, F. Petraki, S. Kennou, S.A. Choulis, Org. Electron. 10 (2009) 61.
[22] K. Jeuris, L. Groenendaal, H. Verheyen, F. Louwet, F.C. De Schryver, Synth. Met. 132 (2003) 289.
[23] H.S. Kang, H.S. Kang, J.K. Lee, J.W. Lee, J. Joo, J.M. Ko, M.S. Kim, J.Y. Lee, Synth. Met. 155 (2005) 176.
[24] J.S. Huang, P.F. Miller, J.S. Wilson, A.J. de Mello, J.C. de Mello, D.D.C. Bradley, Adv. Funct. Mater. 15 (2005) 290.
[25] K. Kawano, R. Pacios, D. Poplavskyy, J. Nelson, D.D.C. Bradley, J.R. Durrant, Sol. Energy Mater. Sol. Cells 90 (2006) 3520.
[26] J.K.J. van Duren, J. Loos, F. Morrissey, C.M. Leewis, K.P.H. Kivits, L.J. van IJzendoorn, M.T. Rispens, J.C. Hummelen, R.A.J. Janssen, Adv. Funct. Mater. 12 (2002) 665.
[27] M. Vazquez, J. Bobacka, A. Ivaska, A. Lewenstam, Sens. Actuator B: Chem. 82 (2002) 7.
[28] V. Shrotriya, G. Li, Y. Yao, C.W. Chu, Y. Yang, Appl. Phys. Lett. 88 (2006) 073508.
[29] F. So, D.Y. Kim, J. Subbiah, G. Sarasqueta, H.J. Ding, Irfan, Y.L. Gao, Appl. Phys. Lett. 95 (2009) 093304.
[30] M.D. Irwin, B. Buchholz, A.W. Hains, R.P.H. Chang, T.J. Marks, Proc. Natl. Acad. Sci. USA 105 (2008) 2783.

[31] S. Han, W.S. Shin, M. Seo, D. Gupta, S.J. Moon, S. Yoo, Org. Electron. 10 (2009) 791.
[32] C. Tao, S.P. Ruan, G.H. Xie, X.Z. Kong, L. Shen, F.X. Meng, C.X. Liu, X.D. Zhang, W. Dong, W.Y. Chen, Appl. Phys. Lett. 94 (2009) 043311.
[33] M.Y. Lin, C.Y. Lee, S.C. Shiu, I.J. Wang, J.Y. Sun, W.H. Wu, Y.H. Lin, J.S. Huang, C.F. Lin, Org. Electron. 11 (2010) 1828.
[34] C. Cantalini, M.Z. Atashbar, Y. Li, M.K. Ghantasala, S. Santucci, W. Wlodarski, M. Passacantando, J. Vac. Sci. Technol. A 17 (1999) 1873.
[35] K.M. Coakley, B.S. Srinivasan, J.M. Ziebarth, C. Goh, Y.X. Liu, M.D. McGehee, Adv. Funct. Mater. 15 (2005) 1927.
[36] W.C. Hu, M. Aryal, K. Trivedi, ACS Nano 3 (2009) 3085.
[37] J.J. Wu, A.F. Gross, S.H. Tolbert, J. Phys. Chem. B 103 (1999) 2374.
[38] T.Q. Nguyen, J.J. Wu, V. Doan, B.J. Schwartz, S.H. Tolbert, Science 288 (2000) 652.